

Characterization of Multi-Layer Ceramic Chip Capacitors up to mm-Wave Frequencies for High-Speed Digital Signal Coupling

Tsugumichi SHIBATA^{†(a)}, Fellow and Yoshito KATO^{††*}, Member

SUMMARY Capacitive coupling of line coded and DC-balanced digital signals is often used to eliminate steady bias current flow between the systems or components in various communication systems. A multi-layer ceramic chip capacitor is promising for the capacitor of very broadband signal coupling because of its high frequency characteristics expected from the downsizing of the chip recent years. The lower limit of the coupling bandwidth is determined by the capacitance while the higher limit is affected by the parasitic inductance associated with the chip structure. In this paper, we investigate the coupling characteristics up to millimeter wave frequencies by the measurement and simulations. A phenomenon has been found in which the change in the current distribution in the chip structure occur at high frequencies and the coupling characteristics are improved compared to the prediction based on the conventional equivalent circuit model. A new equivalent circuit model of chip capacitor that can express the effect of the improvement has been proposed.

key words: coupling capacitance, MLCC, high-speed digital signal, mm-waves

1. Introduction

Advances in information technology have promoted the expansion of the data transmission capacity in various communication systems. The AC coupling technique of properly coded digital signals is often used in the communication systems. DC-balanced line codes are used not only in long-distance communication channels but also in board-to-board and chip-to-chip interconnections. The use of signal coupling by a capacitor eliminates steady flow of bias current between systems or components, thereby reducing power consumption and increasing the degree of design freedom for stable operation of each circuit. In order to realize ideal coupling of high-speed digital signals for such applications, a broadband transmission characteristic from the low end to the high end of frequencies is required for the coupling capacitor.

Recent years, Multi-Layer Ceramic chip Capacitors (MLCCs) have been widely utilized as surface-mounted components of printed circuit boards for variety of electronic equipments and systems. The large capacitance with very small chip size has been realized thanks to the technology that enabled to fabricate a huge number of layers in

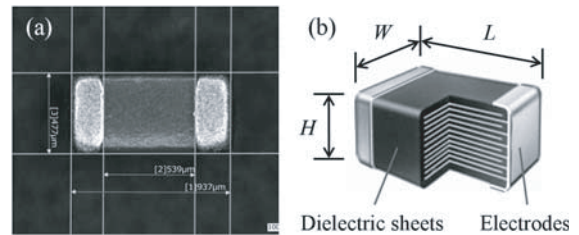


Fig. 1 (a) A photograph of a multi-layer ceramic chip capacitor, and (b) its internal structure.

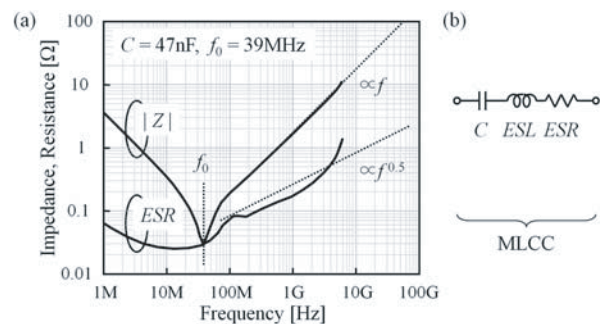


Fig. 2 (a) An example of frequency characteristics of MLCC's impedance Z and equivalent series resistance ESR measured up to 6 GHz [10], and (b) a conventional equivalent circuit model of the MLCC including equivalent series inductance ESL and resistance ESR .

the structure of MLCC, which have been greatly contributed to miniaturize electronic equipments and devices [1], [2]. This reduction in chip size is expected to improve the high-frequency characteristics of capacitors, too. The speed of data transmission handled on the board is increasing from Giga-baud to dozens of Giga-baud level, and the use of the MLCC as the signal coupling (DC blocking) capacitor in these high-speed applications is expected [3]. Therefore, the characteristics of the MLCC up to millimeter-waves become a concern.

Figures 1 (a) and 1 (b) show an enlarged photograph of an MLCC and the schematic of its internal structure. Typical frequency characteristics of MLCC's impedance and equivalent series resistance are illustrated in Fig. 2 (a) and a conventional equivalent circuit model of a capacitor is given in Fig. 2 (b). The self-resonant characteristic of the MLCC due to the parasitic inductance associated with the structure is well known. A series of works have been devoted to increase accuracy of the equivalent circuit model to describe the first self-resonant phenomenon around res-

Manuscript received October 31, 2019.

Manuscript revised February 17, 2020.

Manuscript published April 9, 2020.

[†]The author is with Tokyo City University, Tokyo, 158-8557 Japan.

^{††}The author was with Tokyo City University, Tokyo, 158-8557 Japan.

*Presently, with Mitsubishi Electric Engineering Co., Ltd.

a) E-mail: tshibata@tcu.ac.jp

DOI: 10.1587/transele.2019ESP0004

onant frequency f_0 [4]–[9], and the S -parameters of MLCCs up to around 6 GHz have been measured and published by the manufacturers [10]. Recently, higher order parallel resonance phenomena were investigated using relatively large-size and small-capacitance packages [11]. However, the performance beyond 10 GHz is not adequately studied yet. Very broadband characteristics of MLCCs when used for the signal coupling up to millimeter-waves need to be revealed.

In this paper, we investigate broadband characteristics of the MLCC for the use in the very high-speed digital signal coupling. We have measured the coupling performance of several types of MLCCs up to 65 GHz, and found that high-dielectric-constant-type MLCCs exhibit very good performance with relatively flat frequency characteristics. In addition, we observed an interesting behavior that shows the improvement of insertion losses at high frequencies. In order to get an understanding of the mechanism of the behavior, full-wave electromagnetic field analyses were performed. The 3-dimensional full-wave simulation enables analysis of the behavior with effects including the surface-mounted structure on the circuit board, which cannot be considered in the conventional parallel plate transmission line model analysis [7], [8], and provides a visual understanding of internal electromagnetic field and current distributions. Based on the measurement and analyses, a new equivalent circuit model to describe the characteristics is proposed.

In the next section, the basic coupling performance predicted from the conventional equivalent circuit model is briefly described. Sections 3 and 4 illustrate the measurement and the field analyses, respectively. A new equivalent circuit model is presented in Sect. 5, and Sect. 6 offers concluding remarks.

2. Basic Coupling Characteristics of the MLCC

As seen in Fig. 2 (a), the measured impedance exhibits the self-resonant characteristic at the frequency f_0 that is expressed by

$$f_0 = \frac{1}{2\pi\sqrt{C \times ESL}} \quad (1)$$

where C is the capacitance and ESL is the parasitic equivalent series inductance described in the equivalent circuit model of Fig. 2 (b). Table 1 lists the MLCCs used for the investigation in this paper. Here we choose three high-dielectric-constant-type MLCCs of different sizes.

Note that the chip size may be expressed in inches in some literatures, but in this paper, it is expressed in metric

Table 1 The MLCC samples investigated in this paper.

	Size $L \times W \times H$	Capacitance C	Self-resonant freq. f_0	Inductance ESL
#1	1.0×0.5×0.5mm	47 nF	39 MHz	0.35 nH
#2	0.6×0.3×0.3mm	4.7 nF	140 MHz	0.28 nH
#3	0.4×0.2×0.2mm	4.7 nF	220 MHz	0.11 nH

system. We selected the small ones in size. The sample #1 has the nominal capacitance value of 47 nF and the size is $1.0 \times 0.5 \times 0.5$ mm whereas the samples #2 and #3 have the value of 4.7 nF and smaller sizes of $0.6 \times 0.3 \times 0.3$ and $0.4 \times 0.2 \times 0.2$ mm, respectively. The self-resonant frequencies f_0 obtained from the manufacturer's data sheets and the series inductances ESL calculated using Eq. (1) are also listed. The parasitic ESL ranges between 0.1 nH and 0.4 nH, and it can be seen that the smaller the chip size, the smaller the ESL .

Now let us examine the characteristics of the coupling capacitor that is expressed by the equivalent circuit model of Fig. 2 (b). Imagine the MLCC inserted between 50Ω transmission lines which connect a transmitter circuit at one end and the receiver circuit at the other end. Then, the coupling performance of the MLCC can be evaluated by the two-port S -parameters as illustrated in the inset of Fig. 3. The dependence of the values C and ESL on the frequency characteristics of the insertion loss $|S_{21}|$ is schematically drawn in Fig. 3. Since the MLCC is inserted in series in the line, good signal coupling characteristics are obtained in a frequency band where the impedance of the MLCC is sufficiently small compared to the characteristic impedance of line. It is shown in this figure that the cutoff frequency at the low-end of the bandwidth stems from the value of the capacitance C while that of the high-end of the bandwidth is determined by the inductance ESL . The larger the capacitance C , the lower the low-end of the bandwidth. And the smaller the inductance ESL , the higher the high-end of the bandwidth. Consequently, recent advances in making larger capacitance and smaller chip size of the MLCC should be very attractive for the use in the broadband high-speed digital signal coupling applications. The series resistance ESR was set to 1Ω in the insertion loss simulation of Fig. 3, which had negligibly small effect on the results. However, ESR tends to increase with increasing frequency and can cause degradation of insertion loss at microwave and mm-wave frequencies.

In order to confirm the coupling performance of MLCCs at high frequencies above 10 GHz, we carried out

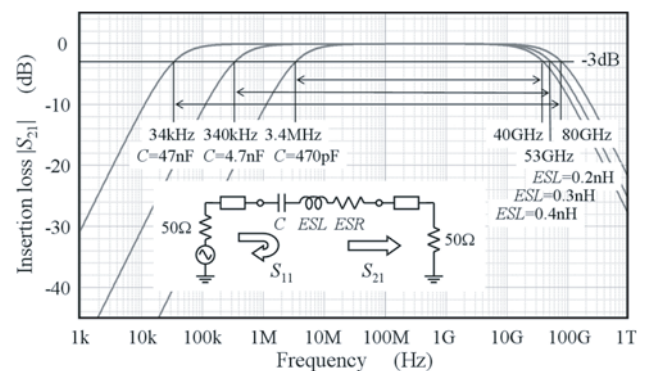


Fig. 3 Frequency characteristics of the insertion loss S_{21} of signal coupling calculated by the conventional equivalent circuit model. The cutoff frequency at low-end depends on the value of the capacitance C while that at high-end is determined by the equivalent series inductance ESL .

the measurement of the insertion and return losses up to 65 GHz.

3. Measurement Results

For the measurement, we need to prepare high-performance fixtures (substrates) that can withstand millimeter-wave frequency operations. In this study, a high temperature co-fired ceramic (HTCC) substrate with surface metal patterns was designed and fabricated for this purpose. The substrate used here is a single plate HTCC with a relative dielectric constant of $\epsilon_r = 9.0$ and a thickness of $T = 0.15$ mm after sintering. The metal layer made of W-Au forms microstrip lines (MSLs) of the width $w = 0.16$ mm that have the characteristic impedance of $Z_0 = 50 \Omega$. Figure 4 shows the measured S -parameters of 2.4 mm-long line with probing pads added at both ends. As can be seen, very good transmission performance with the insertion loss of less than 0.9 dB up to 65 GHz was obtained.

The MLCC samples listed in Table 1 were surface-mounted on the substrate. The layout (the top view) of each sample is illustrated in Fig. 5 (a), 5 (b) and 5 (c). Probing pads for the G-S-G type probe head are provided at the both ends of left- and right-hand sides, where the ground pads are connected to the back metal plane of the substrate via through holes. The S -parameters of these samples were measured on a probe station as shown in Fig. 6 using a vector network analyzer, too. Since the coupling characteristics at high frequencies are considered to depend on not only the capacitor itself but also the mounting structure, we decided to define reference planes in the middle of the MSLs and perform two-port modeling of the mounted MLCC between the reference planes as shown by “Ref.1” and “Ref.2” in Fig. 5. In order to compensate for the transmission loss of the MSLs outside the reference planes, the “through” patterns that have only a MSL with a length excluding the distance between the reference planes was prepared, and these portions were de-embedded using measured S -parameters [12]. Since the through lines showed very good matching with 50Ω characteristic impedance, de-embedding was done by just subtracting the line losses from the total insertion and return losses as shown in the follow-

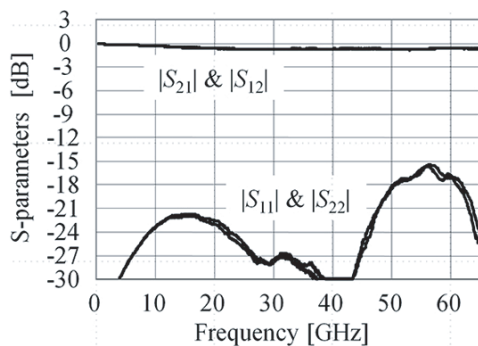


Fig. 4 Measured S parameters of a microstrip line on the HTCC substrate with the line length (pad to pad) of 2.4 mm.

ing equations,

$$\text{Insertion Loss} = 20 \log_{10} \frac{|S_{21, \text{total}}(\omega)|}{|S_{21, \text{line}}(\omega)|} \quad (2)$$

$$\text{Return Loss} = 20 \log_{10} \frac{|S_{11, \text{total}}(\omega)|}{|S_{21, \text{line}}(\omega)|} \quad (3)$$

where, the subscript “total” means the S -parameter of the entire structure including the MLCC, and “line” indicates the S -parameter of the “through” pattern.

The results are plotted in Figs. 7 (a), 7 (b), and 7 (c), respectively. In the figures, the performances predicted from the conventional equivalent circuit model presented in Fig. 2 (b) are also plotted by the dotted lines. As can be seen, the measurement results do not agree well with the predictions of the equivalent circuit model. The measured inser-

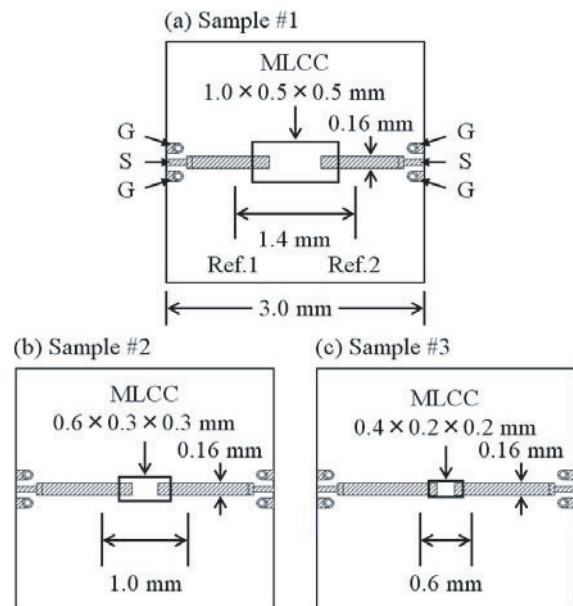


Fig. 5 The layout of MLCC samples mounted on an HTCC substrate. The microstrip line configuration is used for the transmission lines from the MLCC to the both end of probing pads.

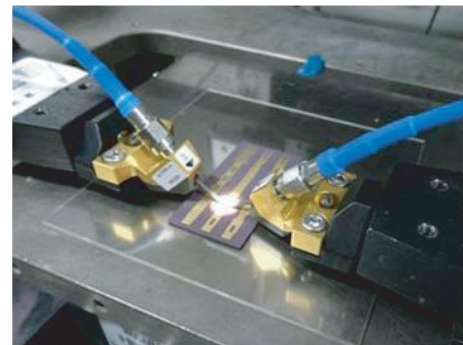


Fig. 6 Photograph of the measurement setup. The samples are probed using the probe heads APC65-A-150(GSG) of Cascade Microtech, Inc.. Two-port S -parameter measurements were carried out using the vector network analyzer N5247APNA-X.

tion loss of these samples begins to increase around 10 or 20 GHz. However, it has little change after that, and it seems to improve somewhat at millimeter-wave frequencies. The behavior of these results can not be explained by the conventional equivalent circuit model. The discrepancy in the return loss is also remarkable. Since the performance at high frequencies depends not only on the characteristics of the MLCC itself but also on mounting conditions, we also fabricated similar samples using a coplanar waveguide structure as the mounting substrate. As the result, the similar behavior as presented in Figs. 7 was observed [13]. Therefore, we conducted full-wave electromagnetic field simulations to verify the credibility of the experimental results and to elucidate the mechanism. Next, we will describe the electromagnetic field simulations of MLCCs.

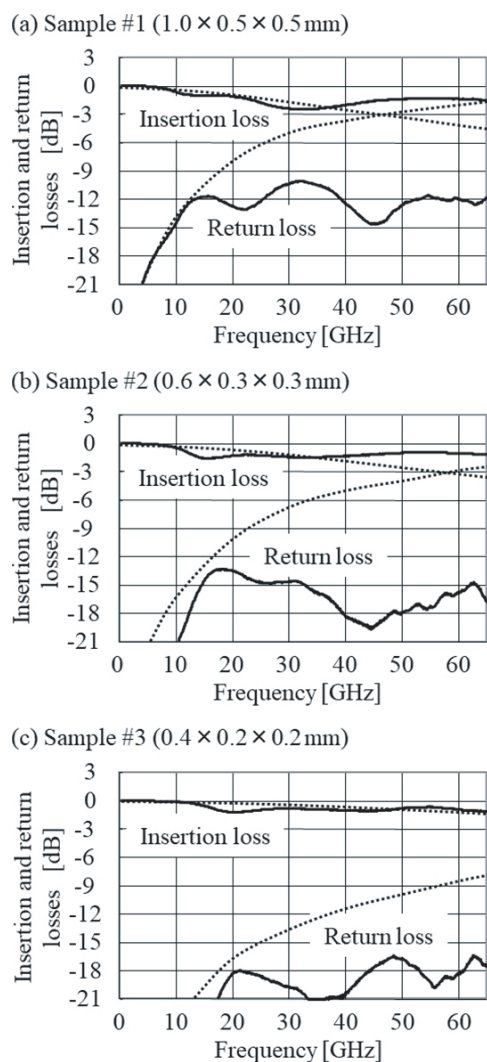


Fig. 7 Measured insertion losses and return losses versus predicted ones using the conventional equivalent circuit model. (a) for sample #1, (b) for sample #2, and (c) for sample #3. The solid lines plot the measured results while the dotted lines show the prediction by the equivalent circuit model presented in Fig. 2 (b).

4. The Full-Wave Analysis of MLCC's Coupling Characteristics

We analyzed the coupling characteristics of MLCCs using a commercially available electromagnetic field solver based on the finite element method [14]. The 3D structures of the MLCC surface-mounted on the substrate as shown in Figs. 5 (a), 5 (b) and 5 (c) were built in a simulation space of $2.4 \times 2.4 \times 2.4$ mm. The MLCC was modeled as schematically illustrated in Fig. 8, which has an internal structure of stacked parallel plate electrodes and thin dielectric sheets. Details of the structure were modeled by inferring from the manufacturer's data sheet and some structural parameters for samples #1 to #3 are summarized in Table 2. Depending on the orientation of the MLCC when mounted on the substrate, two structures as shown in Figs. 9 (a) and 9 (b) can be considered. One is a structure in which the chip is mounted so that its internal electrode layer is parallel to the substrate. And the other is a structure in which the internal electrode layer is perpendicular to the substrate. Consequently, we carried out the analyses and compared these two structures.

S-parameters between the two port-walls were calculated by the simulator. Figure 10 shows the obtained insertion losses $|S_{21}|$ and return losses $|S_{11}|$. From these results, it can be confirmed again that the miniaturization of MLCC is effective in improving the losses. And if you look at the behavior of the insertion losses, it is interesting that they degrade around 10 or 20 GHz, but do not change much after

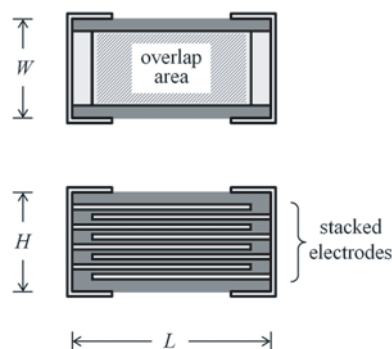


Fig. 8 Schematic diagram of the MLCC structure for 3D electromagnetic full-wave simulations. Thin internal electrodes and dielectric sheets having a high relative permittivity of $\epsilon_r = 8,000$ are stacked. The number of stacked layers and the dielectric thickness are determined so that the parallel plate capacitance of the overlap area becomes the nominal capacitance value.

Table 2 Parameters of simulation models.

	Number of stacked electrodes	Dielectric thickness	Electrode thickness	Overlapping area
#1	24	10.4 μm	3 μm	0.300 mm ² (0.80 \times 0.375 mm)
#2	10	14.7 μm	2 μm	0.108 mm ² (0.48 \times 0.225 mm)
#3	14	9.4 μm	1 μm	0.048 mm ² (0.32 \times 0.150 mm)

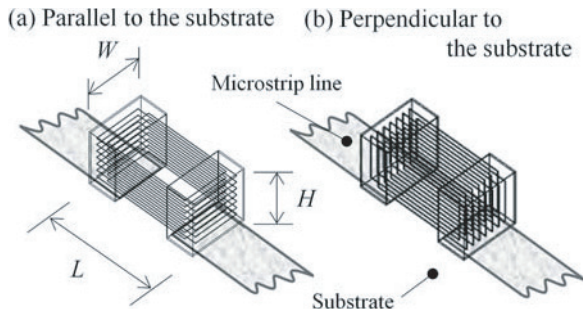


Fig. 9 Two structures of simulation models. The layer of internal electrodes in the MLCC is (a) parallel to, and (b) perpendicular to the substrate. These figures are drawn based on the simulation structure data of sample # 3. The field analyses were performed in an analysis area of $2.4 \times 2.4 \times 2.4$ mm with the analysis scale of 123 k elements of the finite element method.

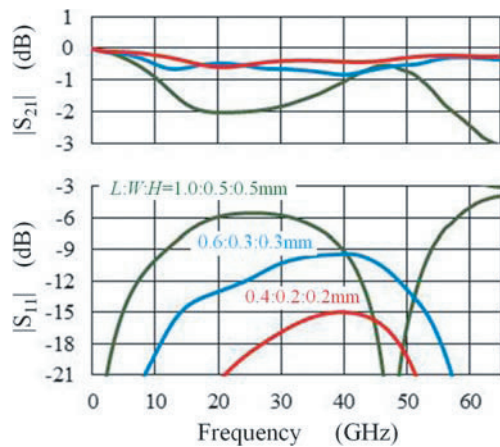


Fig. 10 Calculated results of the insertion and return losses by the full-wave simulations. Green lines for the sample #1 (the MLCC size is $1.0 \times 0.5 \times 0.5$ mm), blue lines for #2 (the size is $0.6 \times 0.3 \times 0.3$ mm), and red lines for #3 (the size is $0.4 \times 0.2 \times 0.2$ mm).

that, and are rather improved at the millimeter wave frequencies. That is, the full-wave simulation results support the experimentally observed behavior quite well. In these simulations, the calculation results of insertion losses and return losses did not show a significant difference between the above-mentioned two structures of different MLCC's orientations.

Figure 11 displays the conduction current distributions in the chip capacitor at frequencies 100 MHz and 10 GHz for all samples. The left column shows the results for the structure in which the internal electrodes are arranged parallel to the surface of the microstrip substrate, and the right column shows those for the structure in which the internal electrodes are perpendicular to the substrate. The intensity of current in the chip structure is indicated by the size and color of arrows in the figure. Comparing the results at the frequencies of 100 MHz and 10 GHz, it can be seen that the current distribution in the chip capacitor changes as the frequency increases. At 100 MHz, the current from the external electrode branches almost uniformly into the internal electrodes

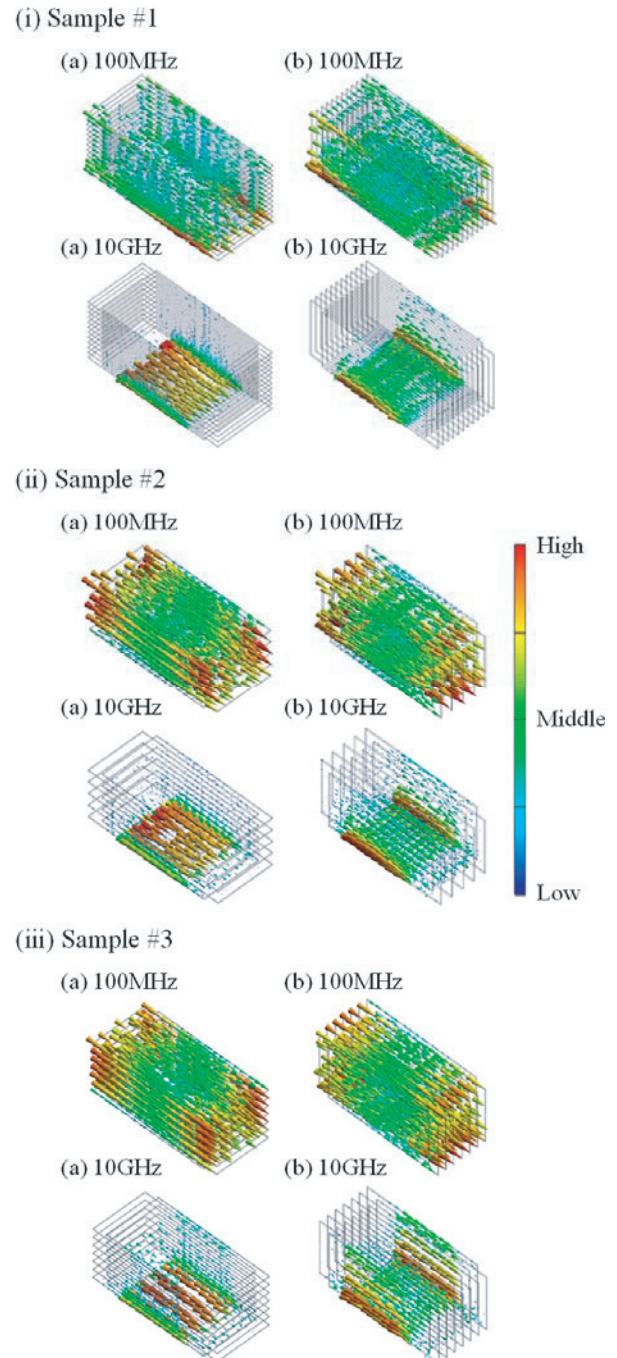


Fig. 11 Calculated current density distributions in the chip capacitor of (i) sample #1, (ii) sample #2, and (iii) sample #3, at frequencies 100 MHz and 10 GHz, respectively. The intensity distribution of the instantaneous conduction current is represented by the size and color of the arrows. (a) is the case that the internal electrode layer is parallel to the substrate, and (b) is the case that the internal electrode layer is perpendicular to the substrate.

and flows evenly through the multilayer electrodes inside the chip of all samples. However, on the other hand, at 10 GHz, the current flows concentrated in a portion close to the microstrip substrate. That is, a change occurs in the current distribution inside the MLCC in this frequency range. This change in the current distribution can be explained in a way

that the impedance for the displacement current between the opposing internal electrodes decreases in inverse proportion to the increased frequency, and a sufficiently large current becomes to pass through only a part of the capacitance component. It may be considered that this change of current distribution causes the improvement of insertion and return losses at millimeter wave frequencies. One can say that the current tends to flow in the shortest path at high frequencies, resulting in a smaller equivalent series inductance component. Considering the change in the current distribution in the MLCC structure, the modified equivalent circuit model of the MLCC is created next.

5. Proposal of a New Equivalent Circuit Model

In order to incorporate the mechanism of the current distribution change into circuit level simulations, we propose a new equivalent circuit model for the capacitor as shown in Fig. 12 (a). In this model, an additional path composed of C_{HF} , L_{HF} , and R_{HF} is added to the previous model. By appropriately selecting the values of parameters C_{HF} , L_{HF} , and R_{HF} , current components having low frequencies can flow through the conventional path including C , ESL , and ESR , while most of high-frequency components flow through the newly added path. Since the capacitor sample #3 having the smallest size was the best as the coupling capacitance of broadband signals up to millimeter-wave frequencies, an attempt was made to calculate the characteristics of sample #3 using the proposed equivalent circuit model. The insertion loss and the return loss of the sample #3, calculated by the proposed model are plotted by the dotted lines in Fig. 12 (b). The new model explains the characteristic behavior at the

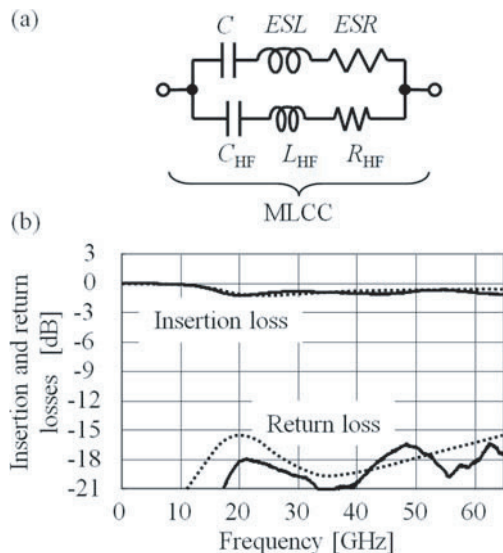


Fig. 12 (a) Proposed new equivalent circuit model, and (b) comparison of measured insertion loss and return loss with the prediction using the proposed equivalent circuit model. The solid lines show the measured results of sample #3, while the dotted lines plot the prediction by the new equivalent circuit model with $C = 4.7$ nF, $ESL = 0.11$ nH, $ESR = 1$ Ω , $C_{HF} = 300$ fF, $L_{HF} = 0.08$ nH, and $R_{HF} = 15$ Ω .

millimeter wave frequencies and agrees with the measured result very well.

The parameters C_{HF} , L_{HF} , and R_{HF} are fitting parameters determined from the measurement data and/or the full-wave simulation results. In this study, these parameters were determined according to the following guidelines. First, the value of C_{HF} is determined so that the magnitude of the impedance of C_{HF} becomes about 50 Ω at a frequency at which the insertion loss starts to increase. In the case of Fig. 12 (b), selected value of 300 fF yields 50 Ω at 10.6 GHz. At frequencies above this point, the current flowing through the newly added path increases and becomes dominant. Next, the value of L_{HF} is determined so that the resonant frequency of L_{HF} and C_{HF} comes in a frequency region where the increase in insertion loss stops and begins to be improved. In Fig. 12 (b), the resonant frequency becomes 32.5 GHz by setting the value of L_{HF} to 0.08 nH. Finally, the value of R_{HF} is determined so that the characteristics of the equivalent circuit model broadly match the measurement result.

We believe that the proposed model is also applicable to capacitors of larger samples # 1 and # 2. However, due to the large size, strict modeling requires additional considerations such as the stray capacitance of the footprint for the mounting substrate.

6. Conclusion

We have carried the broadband characterization of small size MLCCs intended for the use as the high-speed digital signal coupling capacitor. The two-port S -parameters of several samples were measured up to 65 GHz, which revealed the significant discrepancy between the measured performances and predicted ones by the conventional equivalent circuit model. Full-wave electromagnetic field simulations were also performed to verify the experimental results and to reveal the cause of the discrepancy. Based on the findings from the measurements and field analyses, we have proposed a novel equivalent circuit model that explains the measurement very well. The new model is expected to be useful for the precise circuit simulations for designing various communication systems.

Acknowledgments

The authors wish to thank Mr. Satoshi Tsunashima and Mr. Atsushi Aratake of NTT Laboratories for their fruitful discussions and support in the measurement.

References

- [1] Y. Sakabe, "Multilayer ceramic capacitors," *Current Opinion in Solid State and Materials Science*, vol.2, no.5, pp.584–587, Oct. 1997.
- [2] H. Kishi, Y. Mizuno, and H. Chazono, "Base-Metal Electrode-Multilayer Ceramic Capacitors: Past, Present and Future Perspectives," *JJAP*, vol.42, no.1, pp.1–15, Jan. 2003.
- [3] T. Shibata, S. Kimura, H. Kimura, Y. Imai, Y. Umeda, and Y.

Akazawa, "A Design Technique for a 60 GHz-Bandwidth Distributed Baseband Amplifier IC Module," *IEEE J. Solid-State Circuits*, vol.29, no.12, pp.1537–1544, Dec. 1994.

- [4] Y.L. Li, D.G. Figueroa, J.P. Rodriguez, L. Huang, J.C. Liao, M. Taniguchi, J. Canner, and T. Kondo, "A New Technique for High Frequency Characterization of Capacitors" 48th Electronic Components and Technology Conf., pp.1384–1390, Seattle, USA, May 1998. DOI 10.1109/ECTC.1998.678924
- [5] H. Kwak, H. Ke, B.H. Lee, and T. Hubing, "Plate Orientation Effect on the Inductance of Multi-Layer Ceramic Capacitors" 2007 IEEE Topical Meeting on Electrical Performance of Electronic Packaging, pp.95–98, Atlanta, USA, Oct. 2007. DOI 10.1109/EPEP.2007.4387133
- [6] J.-A. Lee, D. Kim, and Y. Eo, "Circuit Modeling of Multi-Layer Ceramic Capacitors Using S-Parameter Measurements," 2008 Int. SoC Design Conf., pp.I-358 - I-361, Busan, Korea, Nov. 2008. DOI 10.1109/SOCD.2008.4815646
- [7] M.-G. Kim, B.H. Lee, and T.-Y. Yun, "Equivalent-Circuit Model for High-Capacitance MLCC Based on Transmission-Line Theory," *IEEE Trans. Comp., Packag. Manuf. Technol.*, vol.2, no.6, pp.1012–1020, June 2012.
- [8] J. Jeon, H. Lee, B. Pu, J.-H. Kim, N. Zhang, and W. Nah, "Prediction of Impedance Characteristics of MLCC Using Multiconductor Transmission Line Theory," *IEEE Trans. Electromagn. Compat.*, vol.58, no.6, pp.1760–1771, Dec. 2016.
- [9] H. Stimac, R. Blečić, R. Gillon, and A. Baric, "Frequency-Domain Characterization and Modelling of a Multi-Layer Ceramic Capacitor for RF Applications," 2019 Joint Int. Symp. Electromagn. Compat. and Asia-Pacific Electromagn. Compat., WedAM1B.1, pp.285–288, Sapporo, Japan, June 2019.
- [10] S-parameters measured by the manufacturers, the data of GRM155B11C473KA01, <http://www.murata.com/ja-jp/tool/sparameter/mlcc>
- [11] H. Patel, L. Levesque, H. Morales, and L. Dunleavy, "Addressing Performance Differences in Horizontal and Vertical Orientation Mounting of Multi-Layer Capacitors," 18th Wireless and Microwave Technology Conf., Cocoa Beach, USA, April 2017. DOI 10.1109/WAMICON.2017.7930261
- [12] J. Song, F. Ling, G. Flynn, W. Blood, and E. Demircan, "A de-embedding technique for interconnects," 10th Topical Meeting on Electrical Performance of Electronic Packaging, Cambridge, USA, Oct. 2001. DOI 10.1109/EPEP.2001.967628
- [13] Y. Kato and T. Shibata, "Broadband Characteristics of Multi-Layer Ceramic Chip Capacitors for High-Speed Digital Signal Coupling," 2018 Asia-Pacific Microwave Conf., TH2-C2-2, Kyoto, Japan, Nov. 2018. DOI 10.23919/APMC.2018.8617246
- [14] Murata Software, <https://www.muratasoftware.com/products/>



Tsugumichi Shibata graduated from the Tokyo National College of Technology in 1980 and received the B.S., M.S., and Ph.D. degrees in electrical engineering from the University of Tokyo in 1983, 1985, and 1995, respectively. In 1985, he joined NTT corporation, where he engaged in research on electromagnetic-field analyses and high-speed integrated circuits for large-capacity data transmission systems. In 2015, he moved to the Tokyo City University, and is now a professor of the faculty of engineering. He was

a Visiting Scholar at the University of California at Los Angeles (UCLA) from 1996 to 1997, and a visiting professor at the Hokkaido University in the fiscal year of 2013. He was the chair of the Microwave Simulator Technical Group of the IEICE from 2003 to 2005, a vice president of the IEICE Electronics Society from 2007 to 2009, the chair of the Electronics Simulation Technical Group from 2012 to 2014, and is now the president of the Electronics Society. He had been serving as an Executive Committee member of the VLSI Symposia from 2007 to 2012 and a member of the APMC Japanese National Committee from 2012 to 2014. He is a member of IEEEJ and a senior member of IEEE.



Yoshito Kato received the B.S. and M.S. degrees in Information and Communication Engineering from Tokyo City University in 2017 and 2019, respectively. He had been engaged in research on the analysis of multi-layer ceramic chip capacitors for microwave and millimeter wave applications. He joined Mitsubishi Electric Engineering Co., Ltd. in 2019.